Manuscript submitted to
AIMS' Journals
Volume **X**, Number **0X**, XX **200X**

Website: http://AIMsciences.org

pp. **X–XX**

ON INITIAL-BOUNDARY VALUE PROBLEMS FOR A BOUSSINESQ SYSTEM OF BBM-BBM TYPE IN A PLANE DOMAIN

V. A. Dougalis

Department of Mathematics, University of Athens
15784 Zographou Greece
and
Institute of Applied and Computational Mathematics
FO.R.T.H.
P.O. Box 1385, 71110 Heraklion, Greece

D. E. Mitsotakis

Department of Mathematics, University of Athens
15784 Zographou Greece
and
Institute of Applied and Computational Mathematics
FO.R.T.H.
P.O. Box 1385, 71110 Heraklion, Greece

J.-C. Saut

UMR de Mathématiques, Université de Paris-Sud
Bâtiment 425
P.O. Box 91405
Orsay, France

(Communicated by Aim Sciences)

Abstract. We consider a Boussinesq system of BBM-BBM type in two space dimensions. This system approximates the three-dimensional Euler equations and consists of three coupled nonlinear dispersive wave equations that describe propagation of long surface waves of small amplitude in ideal fluids over a horizontal bottom. We show that the initial-boundary value problem for this system, posed on a bounded smooth plane domain with homogeneous Dirichlet or Neumann or reflective (mixed) boundary conditions, is locally well-posed in H^1. After making some remarks on the temporal interval of validity of these models, we discretize the system by a standard Galerkin-finite element method and present the results of some numerical experiments aimed at simulating two-dimensional surface wave flows in complex plane domains with a variety of initial and boundary conditions.

2000 *Mathematics Subject Classification.* 35Q53, 76B15, 65M60.

Key words and phrases. Boussinesq systems, BBM-BBM, initial-boundary value problems.

This research was supported in part by a French-Greek scientific cooperation grant jointly by EGIDE, France, and the General Secretariat of Research and Technology, Greece.

1. **Introduction.** In this paper we will study the Boussinesq system

$$\begin{aligned} &\eta_t + \nabla\cdot\mathbf{v} + \nabla\cdot\eta\mathbf{v} - b\Delta\eta_t = 0,\\ &\mathbf{v}_t + \nabla\eta + \tfrac{1}{2}\nabla|\mathbf{v}|^2 - d\Delta\mathbf{v}_t = 0, \end{aligned} \tag{1}$$

where b, d are positive parameters. This system is of the type of Boussinesq systems derived in [5] as approximations to the three-dimensional Euler equations describing irrotational free surface flow of an ideal fluid over a horizontal bottom. The independent variables $\mathbf{x} = (x, y)$ and t represent the position and elapsed time, respectively, $\eta = \eta(\mathbf{x}, t)$ is proportional to the deviation of the free surface from its rest position, while $\mathbf{v} = \mathbf{v}(\mathbf{x}, t) = (u(\mathbf{x}, t), v(\mathbf{x}, t))$ is proportional to the horizontal velocity of the fluid at some height. Specifically, for the systems derived in [5] we have $b = d = \frac{1}{2}(\theta^2 - \frac{1}{3})$, $\frac{1}{3} < \theta^2 \leq 1$; the so-called BBM-BBM system corresponds to $\theta^2 = \frac{2}{3}$, i.e. to $b = d = \frac{1}{6}$. The variables in (1) are nondimensional but unscaled. If z denotes the nondimensional depth variable, then the bottom of the channel lies at $z = -1$, while the horizontal velocity $\mathbf{v}$ is evaluated at height $z = -1+\theta(1+\eta(\mathbf{x}, t))$.

The Boussinesq approximation on which (1) is based is valid when $\varepsilon := A/h_0 << 1$, $\lambda/h_0 >> 1$, and the Stokes number $S := \frac{A\lambda^2}{h_0^3}$ is of order 1; here A is the maximum amplitude of the wave above the undisturbed level of the fluid of depth h_0 and λ is a characteristic wavelength. If one takes $S = 1$ and switches to scaled, nondimensional variables, one may derive from the Euler equations, cf. [5], by appropriate expansion in powers of ε, a scaled version of (1), namely

$$\begin{aligned} &\eta_t + \nabla\cdot\mathbf{v} + \varepsilon(\nabla\cdot\eta\mathbf{v} - b\Delta\eta_t) = O(\varepsilon^2),\\ &\mathbf{v}_t + \nabla\eta + \varepsilon(\tfrac{1}{2}\nabla|\mathbf{v}|^2 - d\Delta\mathbf{v}_t) = O(\varepsilon^2), \end{aligned} \tag{2}$$

from which we obtain (1) by unscaling and replacing the right-hand side by zero.

In [6] we considered the Cauchy problem for a class of Boussinesq systems including (1) as a proper subset, and proved that it is well-posed locally in time in suitable Sobolev spaces. In the note at hand we will pose (1) as part of an initial-boundary value problem on a bounded plane domain Ω with sufficiently smooth boundary $\partial\Omega$, and prove in Section 2 local existence of H^1-solutions in the case of homogeneous Dirichlet boundary conditions, i.e. when $\eta = 0$, $u = v = 0$ on $\partial\Omega$, in the case of homogeneous Neumann boundary conditions, i.e. when $\frac{\partial\eta}{\partial n} = 0$, $\frac{\partial u}{\partial n} = \frac{\partial v}{\partial n} = 0$ on $\partial\Omega$, and in the case of reflective (mixed) boundary conditions corresponding to $\frac{\partial\eta}{\partial n} = 0$, $u = v = 0$ on $\partial\Omega$. (Here $\mathbf{n}$ is the normal direction to the boundary.) These boundary conditions are of some physical relevance. For example, nonhomogeneous in general, Dirichlet boundary conditions for η and $\mathbf{v}$ at the boundary $\partial\Omega$ of a bounded (perhaps artificial) domain could represent experimental measurements of η and $\mathbf{v}$ made at $\partial\Omega$ as functions of t. These data may be used then as boundary conditions for a numerical scheme whose results in the interior of Ω may be compared with experimental values in order to assess the accuracy of the Boussinesq model. Here, the homogeneous boundary conditions are treated as a first step towards the analysis of the nonhomogeneous problem. The reflective boundary conditions are needed for the simulation of water waves colliding with and reflected from solid walls that are perpendicular to the direction of propagation, while the homogeneous Neumann conditions, used in parts of the boundary, are appropriate as side conditions for simulating waves propagating in a direction parallel to the boundary. In addition they may be used as first approximations of outflow (radiation) conditions at open, artificial boundaries.

We would also like to mention that the initial-boundary value problem for the analogous BBM-BBM system in one space dimension with nonhomogeneous Dirichlet boundary conditions at the endpoints of a finite interval was shown to be locally well-posed by Bona and Chen, [3]. Various initial-boundary value problems on a bounded interval for the Bona-Smith family of Boussinesq systems were studied in [2].

When we consider the scaled problem (2) – with zero right-hand side – our existence proof yields local well-posedness on a temporal interval $[0, T_\varepsilon]$ dependent on ε. In the case of homogeneous Dirichlet and reflective boundary conditions we will use an energy argument in Section 2 to prove that actually T_ε is independent of ε. This is not very satisfactory for modelling purposes, since the physically relevant temporal regime for (2) is from $O(1/\varepsilon)$ to $O(1/\varepsilon^2)$. (For the Cauchy problem we proved in [6] that $T_\varepsilon = O(1/\varepsilon^\alpha)$, for any $\alpha < 1/2$. It is worth mentioning that the Cauchy problem for the class of *fully symmetric* Boussinesq systems derived in [4] has an existence theory for times up to $O(1/\varepsilon)$. We refer to the recent paper [1] for a complete justification of all Boussinesq systems.) In the case of homogeneous Neumann boundary conditions the energy proof argument fails and we cannot show that T_ε is independent of ε.

We close the paper by showing the results of three numerical experiments that we performed solving the system (1) numerically, in complex domains under various initial and boundary conditions. We used a fully discrete Galerkin-finite element method with continuous piecewise linear elements on a general triangulation of Ω and a simple explicit time-stepping scheme (The analogous semidiscrete scheme was analyzed in [6] and shown to possess optimal-order rate of convergence in L^2 and H^1 under certain hypotheses.) Our conclusion is that the proposed numerical scheme is stable and efficient and may be used to simulate surface water wave phenomena that are modelled by the Boussinesq system (1).

2. **Well-posedness of the Boussinesq system (1).** We consider the system (1) in its scaled form

$$\begin{aligned} &\eta_t + \nabla\cdot\mathbf{v} + \varepsilon(\nabla\cdot\eta\mathbf{v} - b\Delta\eta_t) = 0,\\ &\mathbf{v}_t + \nabla\eta + \varepsilon(\tfrac{1}{2}\nabla|\mathbf{v}|^2 - d\Delta\mathbf{v}_t) = 0, \end{aligned} \tag{3}$$

for $\mathbf{x} = (x, y) \in \Omega$, $t > 0$, where Ω is a smooth bounded open set in $\mathbb{R}^2$, and $b, d > 0$. We supplement (3) with the initial data

$$\eta(\mathbf{x}, 0) = \eta_0(\mathbf{x}), \quad \mathbf{v}(\mathbf{x}, 0) = \mathbf{v}_0(\mathbf{x}), \qquad \mathbf{x} \in \Omega, \tag{4}$$

and the boundary conditions

$$\eta(\mathbf{x}, t) = 0, \quad \mathbf{v}(\mathbf{x}, t) = 0, \qquad \mathbf{x} \in \partial\Omega, \quad t \ge 0. \tag{5}$$

In the sequel we shall use the standard notation H^s, H^1_0 for the usual L^2-based Sobolev spaces of real functions on Ω and put $\mathbf{H}^1_0 = (H^1_0)^2$ etc. We shall also use a Lemma proved by Grisvard, [7], which for plane Lipschitz domains may be stated as follows:

Lemma 2.1. *Let s_1, s_2, $s_3 \in \mathbb{R}$ be such that $s_1 \ge s_3$, $s_2 \ge s_3$, $s_1 + s_2 \ge 0$, $s_1 + s_2 - s_3 > 1$. Then, $(f, g) \mapsto fg$ is continuous from $H^{s_1} \times H^{s_2}$ into H^{s_3}.* □

We write (3) formally as

$$\begin{aligned} &\eta_t + (I - \varepsilon b\Delta)^{-1}\left[\nabla\cdot\mathbf{v} + \varepsilon\nabla\cdot\eta\mathbf{v}\right] = 0,\\ &\mathbf{v}_t + (I - \varepsilon d\Delta)^{-1}\left[\nabla\eta + \varepsilon\tfrac{1}{2}\nabla|\mathbf{v}|^2\right] = 0. \end{aligned} \tag{6}$$

The main result of this section is:

Theorem 2.2. *Let* $(\eta_0, \mathbf{v}_0) \in H_0^1 \times \mathbf{H}_0^1$*. Then, there exists* $T > 0$*, independent of* ε*, and a unique solution* $(\eta, \mathbf{v}) \in C^1([0,T]; H_0^1) \times C^1([0,T]; \mathbf{H}_0^1)$ *of (4), (5), (6).*

Proof. We consider (3) denoting by $(I-\varepsilon b\Delta)^{-1}$, respectively $(I-\varepsilon d\Delta)^{-1}$, the inverse of the operator $I - \varepsilon b\Delta$, respectively $I - \varepsilon d\Delta$, with domain $H^2 \cap H_0^1$, respectively $\mathbf{H}^2 \cap \mathbf{H}_0^1$.

Let $F(\eta, \mathbf{v})$ be the vector field on $H_0^1 \times \mathbf{H}_0^1$ defined by

$$F(\eta, \mathbf{v}) = \left((I - \varepsilon b\Delta)^{-1} \left[\nabla \cdot \mathbf{v} + \varepsilon \nabla \cdot \eta \mathbf{v}\right],\ (I - \varepsilon d\Delta)^{-1} \left[\nabla \eta + \varepsilon \tfrac{1}{2} \nabla |\mathbf{v}|^2\right]\right).$$

F is well-defined in $H_0^1 \times \mathbf{H}_0^1$, since, by the Sobolev imbedding theorem $\eta \mathbf{v} \in \mathbf{L}^2$ and $|\mathbf{v}|^2 \in L^2$; hence, $(I - \varepsilon b\Delta)^{-1}(\nabla \cdot \eta \mathbf{v}) \in H_0^1$ and $(I - \varepsilon d\Delta)^{-1} \nabla |\mathbf{v}|^2 \in \mathbf{H}_0^1$. Moreover, F is C^1 on $H_0^1 \times \mathbf{H}_0^1$, with derivative $F'(\eta^*, \mathbf{v}^*)$ given by

$$\begin{aligned} F'(\eta^*, \mathbf{v}^*)(\eta, \mathbf{v}) &= \big(\varepsilon (I - \varepsilon b\Delta)^{-1} \nabla \cdot (\eta \mathbf{v}^*) + (I - \varepsilon b\Delta)^{-1} [\nabla \cdot \mathbf{v} + \varepsilon \nabla \cdot \eta^* \mathbf{v}], \\ &\quad (I - \varepsilon d\Delta)^{-1} \nabla \eta + \varepsilon (I - \varepsilon d\Delta)^{-1} \nabla (\mathbf{v}^* \cdot \mathbf{v})\big). \end{aligned}$$

The continuity of F' follows from Sobolev imbedding and the regularity properties of the operators $(I - \varepsilon b\Delta)^{-1}$, $(I - \varepsilon d\Delta)^{-1}$.

From the standard theory of ordinary differential equations in Banach spaces, we conclude therefore that there exists a unique maximal solution

$$(\eta, \mathbf{v}) \in C^1([0, T_\varepsilon]; H_0^1) \times C^1([0, T_\varepsilon]; \mathbf{H}_0^1)$$

of (6) with $\eta|_{t=0} = \eta_0$ and $\mathbf{v}|_{t=0} = \mathbf{v}_0$. Applying now $I - \varepsilon b\Delta$ to the first and $I - \varepsilon d\Delta$ to the second equation of (6), we infer that $(\eta, \mathbf{v})$ satisfies (3) in the sense of $H^{-1} \times \mathbf{H}^{-1}$ for $0 < t < T_\varepsilon$.

In order to prove that T_ε may be chosen independent of ε, we use an energy argument. Applying the H^{-1}, H^1 duality of (3) with η, $\mathbf{v}$, we obtain, using the homogeneous Dirichlet boundary conditions

$$\frac{1}{2} \frac{d}{dt} \int_\Omega \left(|\mathbf{v}|^2 + \eta^2 + \varepsilon b |\nabla \eta|^2 + \varepsilon d |\nabla \mathbf{v}|^2\right) = I_\varepsilon := \varepsilon \int_\Omega \eta \mathbf{v} \cdot \nabla \eta + \frac{\varepsilon}{2} \int_\Omega |\mathbf{v}|^2 \nabla \cdot \mathbf{v}, \quad (7)$$

where $|\nabla \mathbf{v}|^2 := |\nabla u|^2 + |\nabla v|^2$. In the sequel, we shall use the notation $\lesssim \cdots$ to denote the inequality $\leq C \cdots$, where C is a positive constant independent of ε, and denote by $\|\cdot\|_p$ the $L^p(\Omega)$ norm. We estimate the right-hand side of (7) as follows. First we have by Hölder's inequality

$$|I_\varepsilon| = \left|\varepsilon \int_\Omega \eta \mathbf{v} \cdot \nabla \eta + \frac{\varepsilon}{2} \int_\Omega |\mathbf{v}|^2 \nabla \cdot \mathbf{v}\right| \lesssim \varepsilon \|\nabla \eta\|_2 \|\mathbf{v}\|_4 \|\eta\|_4 + \varepsilon \|\mathbf{v}\|_4^2 \|\nabla \mathbf{v}\|_2. \quad (8)$$

Using in (8) the Gagliardo-Nirenberg inequality in two dimensions

$$\|f\|_4 \lesssim \|f\|_2^{1/2} \|\nabla f\|_2^{1/2}, \quad f \in H_0^1,$$

we deduce that

$$|I_\varepsilon| \lesssim \varepsilon \|\nabla \eta\|_2^{3/2} \|\eta\|_2^{1/2} \|\mathbf{v}\|_2^{1/2} \|\nabla \mathbf{v}\|_2^{1/2} + \varepsilon \|\mathbf{v}\|_2 \|\nabla \mathbf{v}\|_2^2. \quad (9)$$

From Young's inequality we have

$$\varepsilon \|\mathbf{v}\|_2 \|\nabla \mathbf{v}\|_2^2 \lesssim \varepsilon^2 \|\nabla \mathbf{v}\|_2^4 + \|\mathbf{v}\|_2^2.$$

In addition,

$$\begin{aligned} \varepsilon \|\nabla \eta\|_2^{3/2} \|\eta\|_2^{1/2} \|\mathbf{v}\|_2^{1/2} \|\nabla \mathbf{v}\|_2^{1/2} &\lesssim \varepsilon^2 \|\nabla \eta\|_2^4 + \varepsilon^{2/5} \|\nabla \mathbf{v}\|_2^{4/5} \|\eta\|_2^{4/5} \|\mathbf{v}\|_2^{4/5} \\ &\lesssim \varepsilon^2 \|\nabla \eta\|_2^4 + \varepsilon^2 \|\nabla \mathbf{v}\|_2^4 + \|\eta\|_2^2 + \|\mathbf{v}\|_2^2. \end{aligned}$$

Using these inequalities in (9) we finally obtain

$$|I_\varepsilon| \lesssim \varepsilon^2\|\nabla\eta\|_2^4 + \varepsilon^2\|\nabla\mathbf{v}\|_2^4 + \|\eta\|_2^2 + \|\mathbf{v}\|_2^2. \tag{10}$$

Denoting

$$Y_\varepsilon(t) := \int_\Omega \left(|\mathbf{v}(\cdot,t)|^2 + |\eta(\cdot,t)|^2 + \varepsilon b|\nabla\eta(\cdot,t)|^2 + \varepsilon d|\nabla\mathbf{v}(\cdot,t)|^2\right),\ t \ge 0,$$

we deduce from (7) and (10) that

$$Y_\varepsilon'(t) \lesssim Y_\varepsilon(t) + Y_\varepsilon^2(t),$$

which gives an *a priori* bound of $Y_\varepsilon(t)$ on a time interval $[0, \widetilde{T}_\varepsilon)$ where $\widetilde{T}_\varepsilon = \log\left(1 + \frac{1}{Y_\varepsilon(0)}\right)$. Since

$$Y_\varepsilon(0) = \int_\Omega \left(|\mathbf{v}_0|^2 + |\eta_0|^2 + \varepsilon b|\nabla\eta_0|^2 + \varepsilon d|\nabla\mathbf{v_0}|^2\right),$$

this clearly implies our claim. □

We consider now the case of the reflective boundary conditions

$$\frac{\partial\eta}{\partial n}(\mathbf{x},t) = 0,\ \mathbf{v}(\mathbf{x},t) = 0,\ \mathbf{x} \in \partial\Omega,\ \ t \ge 0. \tag{11}$$

Theorem 2.3. *Let* $(\eta_0, \mathbf{v}_0) \in H^1 \times \mathbf{H}_0^1$*. Then, there exists* $T > 0$*, independent of* ε*, and a unique solution* $(\eta, \mathbf{v}) \in C^1([0,T]; H^1) \times C^1([0,T]; \mathbf{H}_0^1)$ *of (4), (6).*

Proof. The local well-posedness on a time interval $[0, T_\varepsilon]$, $T_\varepsilon > 0$ proceeds exactly as in the proof of Theorem 2.2, but now $(I - \varepsilon b\Delta)^{-1}$ has to be viewed as the inverse of $I - \varepsilon b\Delta$ with Neumann boundary conditions, with domain H^2.

The fact that T_ε does not depend on ε is also proven essentially in the same way as in the pure Dirichlet problem. (The Gagliardo-Nirenberg estimate on $\|\eta\|_4$ has to be replaced by a suitable interpolation estimate.)

Note that although the Dirichlet condition on $\mathbf{v}$ is satisfied since $\mathbf{v} \in \mathbf{H}_0^1$, the Neumann condition on η is only satisfied in a very weak sense, namely $\frac{\partial\eta_t}{\partial n}\Big|_{\partial\Omega} = 0$ in $L^2(\partial\Omega)$. (See also the proof of Theorem 2.4.) □

We consider finally the case of Neumann boundary conditions, i.e.

$$\frac{\partial\eta}{\partial n}(\mathbf{x},t) = 0,\ \frac{\partial\mathbf{v}(\mathbf{x},t)}{\partial n} = 0,\ \mathbf{x} \in \partial\Omega,\ \ t \ge 0. \tag{12}$$

We have

Theorem 2.4. *Let* $(\eta_0, \mathbf{v}_0) \in H^1 \times \mathbf{H}^1$*. Then, there exists* $T_\varepsilon > 0$*, and a unique solution* $(\eta, \mathbf{v}) \in C^1([0,T_\varepsilon]; H^1) \times C^1([0,T_\varepsilon]; \mathbf{H}^1)$ *of (4), (6).*

Proof. The proof proceeds along the lines of the proof of Theorem 2.2. (Note that, by Grisvard's lemma, $\nabla\cdot(\eta\mathbf{v})$, resp. $\nabla|\mathbf{v}|^2$, belongs to H^{s-1}, resp. $\mathbf{H}^{s-1}$, for any $s < 1$. Then $(I - \varepsilon b\Delta)^{-1}\nabla\cdot(\eta\mathbf{v})$, resp. $(I - \varepsilon d\Delta)^{-1}\nabla|\mathbf{v}|^2$, belongs to H^{s+1}, resp. $\mathbf{H}^{s+1}$, and the normal derivative trace $\frac{\partial}{\partial n}$ on η_t, $\mathbf{v}_t$, makes sense in $L^2(\partial\Omega)$ provided $s > 1/2$.) However, in this case the energy proof argument that we used to show that T_ε is independent of ε fails.

Note again the Neumann condition is satisfied only by η_t and $\mathbf{v}_t$. □

Remark 1. The above analysis is valid in the case of more regular initial data. For instance when $(\eta_0, \mathbf{v}_0) \in H_0^1 \cap H^2 \times \mathbf{H}_0^1 \cap \mathbf{H}^2$, the solution of Theorem 2.2 belongs to $C^1([0,T]; H_0^1 \cap H^2) \times C^1([0,T]; \mathbf{H}_0^1 \cap \mathbf{H}^2)$.

Similarly, if $(\eta_0, \mathbf{v}_0) \in H^2 \times \mathbf{H}^2$, and satisfy (11) or (12), the solution obtained in Theorem 2.3 (resp. Theorem 2.4) belongs to $C^1([0,T]; H^2) \times C^1([0,T]; \mathbf{H}^2)$ (resp. $C^1([0,T_\varepsilon]; H^2) \times C^1([0,T_\varepsilon]; \mathbf{H}^2)$) and satisfies the boundary conditions (11) (resp. (12)). This can be checked by performing the Picard iteration procedure in a H^2 setting, with the appropriate boundary conditions.

3. **Numerical experiments.** In this section we present the results of three numerical simulations of nonlinear dispersive surface waves in complex plane domains with a variety of boundary conditions. We solved numerically the BBM-BBM system ($b = d = \frac{1}{6}$ in (1)) using the standard Galerkin-finite element method with continuous, piecewise linear elements on triangles; this scheme was analyzed for the BBM-BBM system with homogeneous Dirichlet boundary conditions in [6] and was shown to converge at the optimal rate 2, respectively 1, in the L^2, respectively H^1, norm provided the solution is sufficiently smooth. (The same error estimates hold in the case of reflective boundary conditions on $\partial\Omega$). In order to construct the finite element triangulation, we used the Matlab PDE toolbox, [8], with three refinements and mesh growth rate equal to 1.01.

The temporal discretization was effected by the 'improved Euler' method, a simple explicit Runge-Kutta scheme of second order of accuracy. (As the o.d.e. system produced by the Galerkin semidiscretization of (1) is not stiff, we may use an explicit method for time-stepping without imposing a restrictive condition on the time step.) The attendant large, sparse linear systems are solved at each time step by the conjugate gradient method with the Jacobi preconditioner.

In the first experiment we consider the unscaled, nondimensional form (1) of the BBM-BBM system. Our domain is the channel $[-15, 15] \times [-30, 50]$ with a vertical, impenetrable cylinder with center at $(0, 10)$ and radius 1.5. We use reflective boundary conditions on the boundary of the cylinder and along the lines $y = -30$ and $y = 50$. On the lines $x = -15$ and $x = 15$ we make use of homogeneous Neumann boundary conditions for both free surface η and velocity components u and v. We use as initial conditions an approximation of a line solitary wave (cf. [6]) of the BBM-BBM system of the form

$$\begin{aligned} &\eta_0(x,y) = A\mathrm{sech}^2\left(\tfrac{1}{2}\sqrt{\tfrac{3A}{c_s}}(y+10)\right), \\ &u_0(x,y) = 0, \\ &v_0(x,y) = \eta_0(x,y) - \tfrac{1}{4}\eta_0^2(x,y), \end{aligned} \tag{13}$$

where $A = 0.1$, $c_s = 1 + \frac{A}{2}$. These initial conditions produce a good approximation of a line solitary wave, which starts at $y = -10$ at $t = 0$ and propagates mainly in the positive y direction travelling with speed $c_s = 1.05$ (cf. Figures 1, 2, 3). The main bulk of the solitary wave travels past the obstacle. Smaller amplitude scattered waves are produced by the interaction of the solitary wave with the obstacle and seem to propagate radially away from it. In this experiment we used 290112 elements and $\Delta t = 1/150$. Similar observations have been made by Wang *et. al.* in [9], for a similar problem in the case of other Boussinesq type equations.

As a second example, we consider the BBM-BBM system with dimensional variables. Our domain represents part of a port of depth $h_0 = 50\,m$ and consists of the rectangle $[-250, 250] \times [0, 2000]$, from which the long rectangular pier

$[0,100]\times[0,700]$ has been removed, cf. Figure 4. (All distances in meters.) Reflective boundary conditions are assumed to hold along the pier and the intervals $[-250,0]$ and $[100,250]$ of the x-axis, while homogenous Neumann boundary conditions for η, u and v have been used on the remaining boundary. An initial wave form with $\eta_0(x,y) = A\exp\left(-\frac{y-1500}{6000}\right)$, $A = 1\,m$, and initial velocity components $u_0(x,y) = 0\,m/sec$, $v_0(x,y) = -\frac{1}{2}\left(\eta_0(x,y) - \frac{1}{4}\eta_0^2(x,y)\right)\,m/sec$, travels mainly towards the negative y direction leaving a dispersive tail behind. (We integrated the system using 77632 elements and $\Delta t = 0.01\,sec$. For the impinging wave we estimated at about $t = 30\,sec$ that $A/h_0 \cong 0.014$, $\lambda/h_0 \simeq 16.6$, so that the Stokes number is approximately $S \simeq 3.9$.) The incoming wave hits the pier and the port boundary at $x = 0$, is reflected backwards and interacts with the pier and the other parts of the boundary. Figure 4 shows a sequence of surface elevation contour plots for this flow up to $T = 2\,min\,40\,sec$. Shown also in Figure 5 are some y-cross sections at $x = -200m$ of the elevation of the wave at several time instances.

In the third example we consider the BBM-BBM system in dimensional form on the plane domain shown in Figure 6 included in a square of size $300\,km$ in an ocean with constant depth $h_0 = 2000\,m$. The computational domain is bounded to the northeast by a continental shoreline curve and includes a small elliptic island. Reflective boundary conditions are applied at the shoreline and the island and Neumann boundary conditions at the open sea boundaries. An initial waveform, resembling an earthquake generated-tsunami, with

$$\eta_0(x,y) = 1 - 1/(1 + 10^3 e^{(-(\frac{-7\cdot 10^4+x-0.2y}{10^4})^2 - (\frac{-13\cdot 10^4+0.2x+y}{10^{7/2}})^2)}) \quad \text{meters},$$

and $u_0 = v_0 = 0\,m/sec$ evolves, and at about $t = 10\,min$ reaches the shoreline and is subsequently reflected backwards. Figure 6 shows contour plots of the evolution of η up to $t = 16\,min\;40\,sec$. (Note that a tsunami travelling with a speed of $\sqrt{gh_0} = 140.07\,m/sec$ would reach the continental shore at about $t = 10min\,7sec$.) The BBM-BBM system was integrated numerically with 133376 elements of maximum size $h \simeq 1500\,m$, and $\Delta t = 0.02\,sec$. In Figure 7 we show the free surface elevation as a function of time at four locations (gauges) in the domain of integration. (This is of course just a toy example intended to test the code, as constant bathymetry has been assumed and the Stokes number, being approximately equal to 0.03 at the beginning of the computation, is too small for modeling purposes.)

REFERENCES

[1] B. Alvarez-Samaniego and D. Lannes, Large time existence for 3D waves and asymptotics, Preprint 2007.

[2] D. C. Antonopoulos, *The Boussinesq system of equations: Theory and numerical analysis*, Ph.D. Thesis, University of Athens, 2000 (in Greek).

[3] J. L. Bona and M. Chen, *A Boussinesq system for two-way propagation of nonlinear dispersive waves*, Physica D, **116**(1998), 191–224.

[4] J. L. Bona, T. Colin and D. Lannes, *Long wave approximations for water waves*, Arch. Rational Mech. Anal., **178**(2005), 373–410.

[5] J. L. Bona, M. Chen, and J.-C. Saut, *Boussinesq equations and other systems for small-amplitude long waves in nonlinear dispersive media: I. Derivation and Linear Theory*, J. Nonlinear Sci., **12**(2002), 283–318.

[6] V. A. Dougalis, D. E. Mitsotakis, and J.-C. Saut, *On some Boussinesq systems in two space dimensions: theory and numerical analysis*, to appear in Math. Model. Num. Anal.

[7] P. Grisvard, *Quelques proprietés des espaces de Sobolev utiles dans l' étude des équations de Navier-Stokes (I)*, Problèmes d' évolution non linéaires, Séminaire de Nice, 1974–1976.

[8] *Partial differential equation toolbox user's guide*, The MathWorks Inc, 2007.

[9] K.-H. Wang, T. Wu and G. T. Yates, *Three-dimensional scattering of solitary waves by vertical cylinder*, J. Waterway, Port, Coastal, and Ocean Eng., **118** (1993),551–565.

E-mail address: doug@math.uoa.gr; dmitsot@math.uoa.gr; jean-claude.saut@math.u-psud.fr

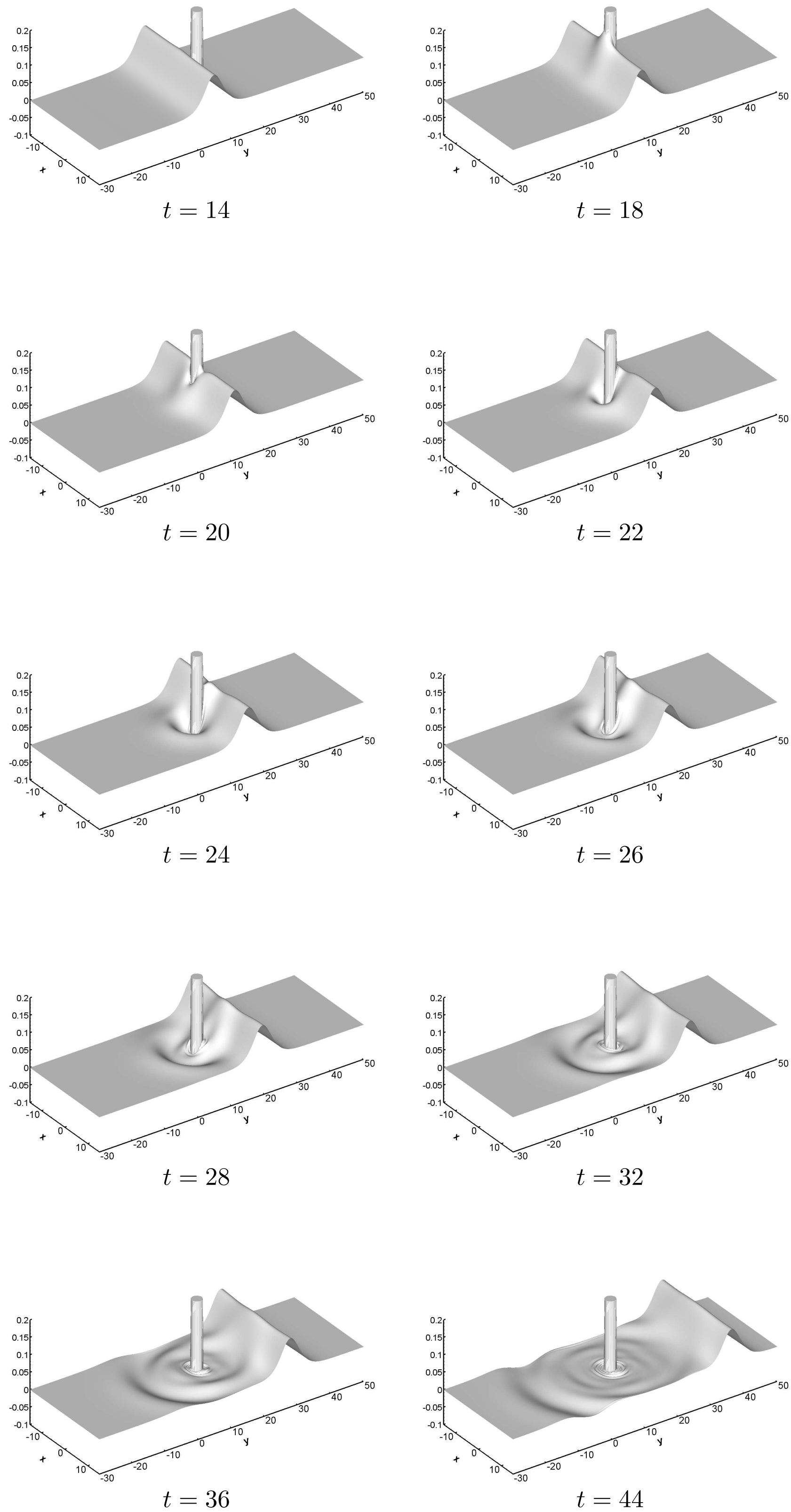

FIGURE 1. Experiment No. 1. Interaction of a line solitary wave with a vertical cylindrical obstacle. Free surface elevation.

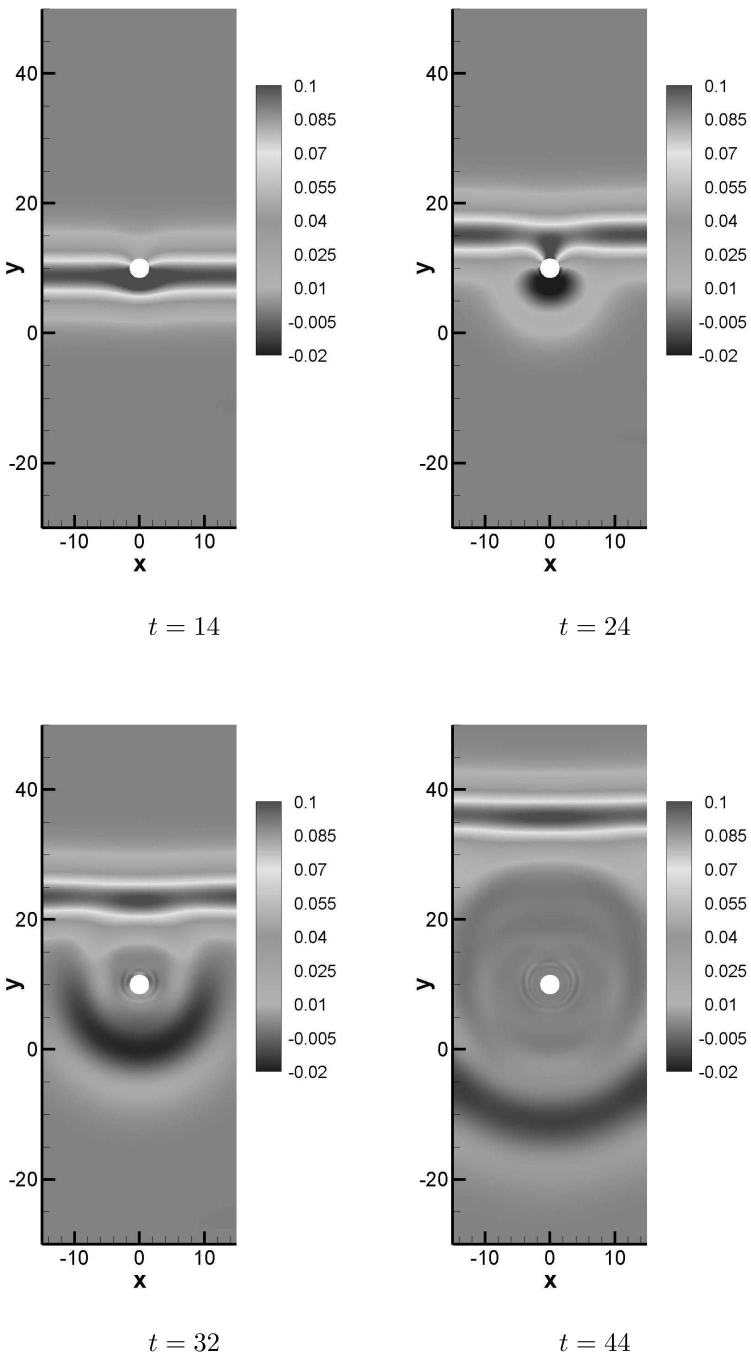

FIGURE 2. Experiment No. 1. Free surface elevation contour plots at four time instances.

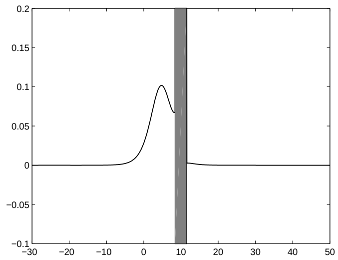

$x = 0, t = 14$

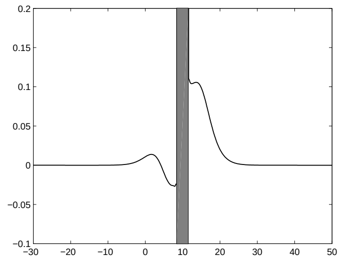

$x = 0, t = 24$

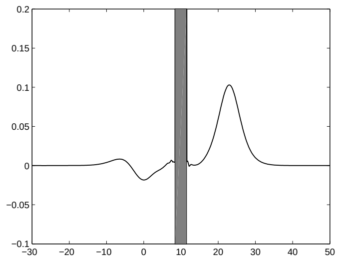

$x = 0, t = 32$

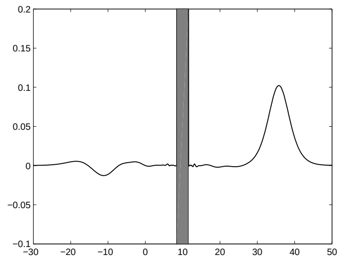

$x = 0, t = 44$

FIGURE 3. Experiment No. 1. One-dimensional plots of free surface elevation along the line $x = 0$ at the time instances of Figure 2.

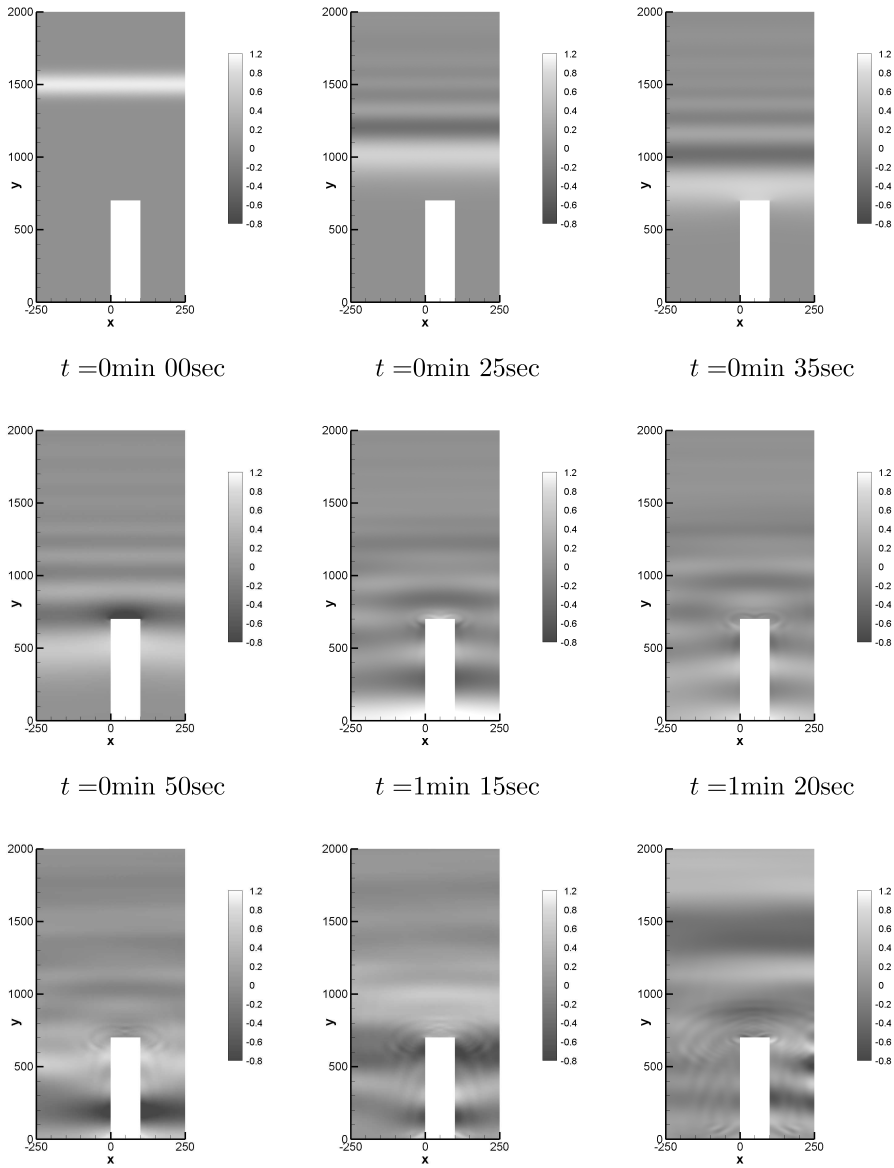

t =0min 00sec t =0min 25sec t =0min 35sec

t =0min 50sec t =1min 15sec t =1min 20sec

t =1min 40sec t =2min 00sec t =2min 40sec

FIGURE 4. Experiment No. 2. Line wave impinging on a port structure. Free surface elevation contour plots. (Distances in meters.)

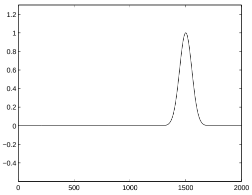

t =0min 00sec

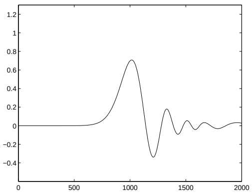

t =0min 25sec

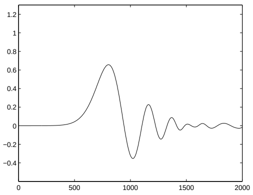

t =0min 35sec

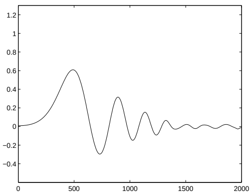

t =0min 50sec

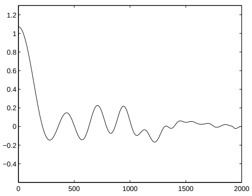

t =1min 15sec

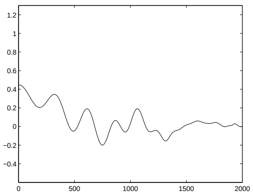

t =1min 20sec

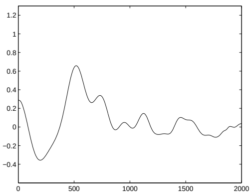

t =1min 40sec

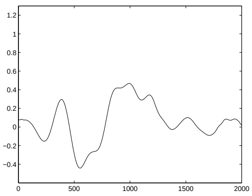

t =2min 00sec

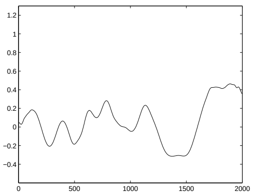

t =2min 40sec

FIGURE 5. Experiment No. 2. Cross sections of η as function of y at $x = -200\,m$ at the time instances of Figure 4. (Distances in meters.)

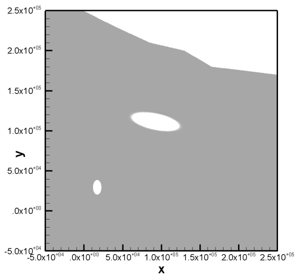

t =0min 00sec

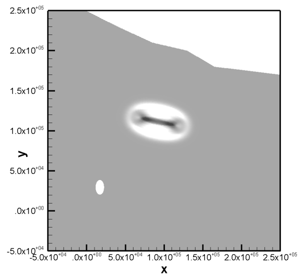

t =1min 40sec

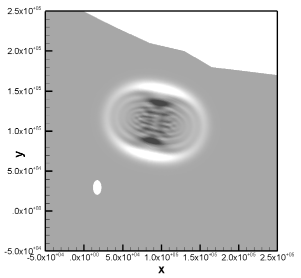

t =5min 00sec

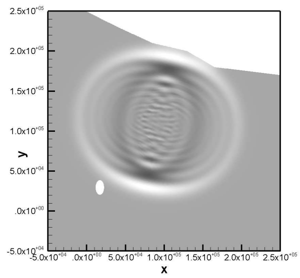

t =10min 00sec

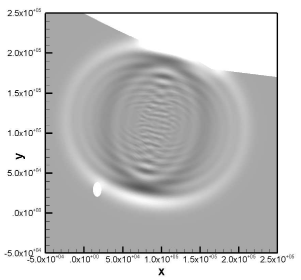

t =11min 40sec

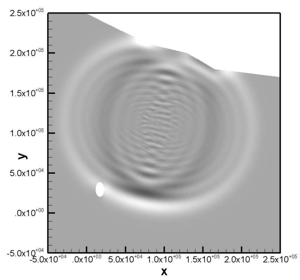

t =12min 20sec

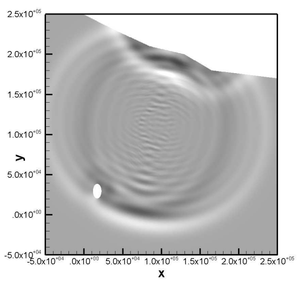

t =15min 00sec

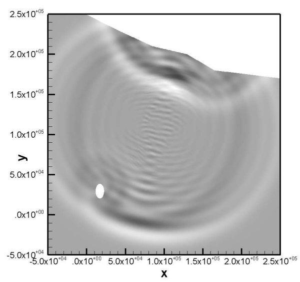

t =16min 40sec

FIGURE 6. Experiment No 3. "Tsunami" wave in a constant depth environment. Free surface elevation contour plots. (Distances in meters.)

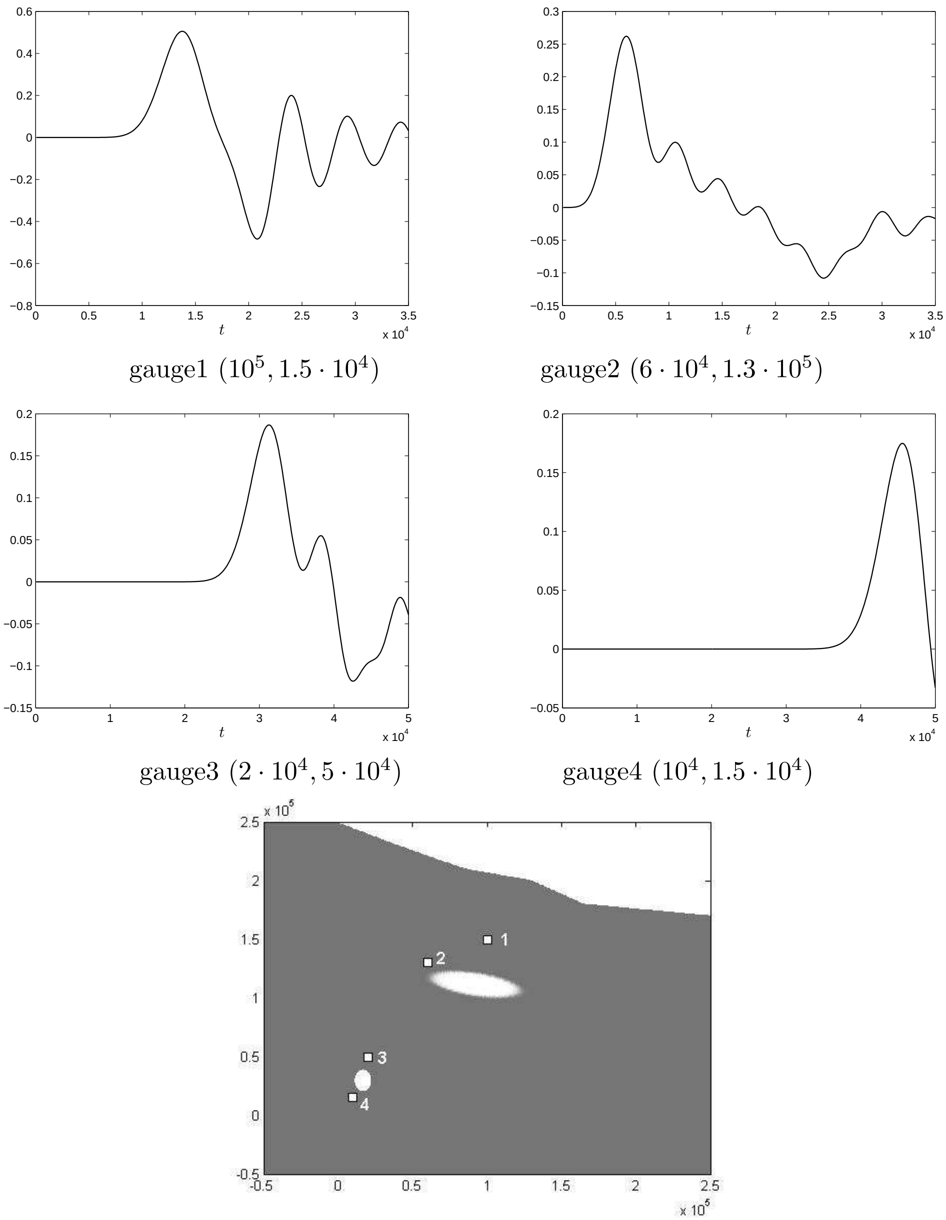

gauge1 $(10^5, 1.5 \cdot 10^4)$

gauge2 $(6 \cdot 10^4, 1.3 \cdot 10^5)$

gauge3 $(2 \cdot 10^4, 5 \cdot 10^4)$

gauge4 $(10^4, 1.5 \cdot 10^4)$

FIGURE 7. Experiment No. 3. Free surface elevation as function of time at the four gauges shown. (Distances in meters.)